



# Chelating agent-free solid phase extraction (CAF-SPE) of uranium, cadmium and lead by Fe-Al-Mn nanocomposite from aqueous solution

Ayalew Manahilie Dinkirie<sup>1,\*</sup> , Abi M. Tadesse<sup>1</sup>, and Tesfahun Kebede<sup>1</sup>

<sup>1</sup>Department of Chemistry, Haramaya University, Haramaya, Ethiopia

**Received:** 9 November 2021

**Accepted:** 6 August 2022

**Published online:**  
25 August 2022

© The Author(s), under exclusive licence to Springer Science+Business Media, LLC, part of Springer Nature 2022

## ABSTRACT

Fe-Al-Mn nanocomposite has been synthesized by impregnating MnO<sub>2</sub> with Fe and Al nitrate aqueous solution for preconcentration and determination of Pb (II), Cd (II) and U (VI) ions from aqueous solution. Fourier Transform Infrared spectroscopy (FTIR), X-Ray-diffraction (XRD) and Scanning electron microscopy coupled with energy dispersive X-ray detector (SEM-EDX) were employed to characterize the as-synthesized nanocomposite. The XRD result indicates that the as-synthesized nanocomposite had a crystal size with rhombohedral structure and size of 30.81 nm. FTIR results confirmed the presence of hydroxyl group and Metal-Oxygen vibration in the adsorbent. A sensitive and simple solid-phase preconcentration procedure for the determination of trace amounts of Pb(II) and Cd(II) ions by FAAS and U(VI) ions by Uv-Vis was developed. The adsorption isotherm was formally described by both Langmuir and Freundlich equation with a maximum adsorption capacity of 12.5 (Pb), 12.8(Cd) and 14.9(U) mg g<sup>-1</sup> respectively with preconcentration factor of 15. The limits of detection were 0.09, 0.05 and 0.0097 mg L<sup>-1</sup> and the relative standard deviation for ten replicate measurements were 2.47, 0.979 and 2.04%, for Pb (II), Cd(II) and U(VI) ions, respectively. The recovery of Pb(II), Cd(II) and U(VI) ions were found to be 92.7, 91.3, and 81.76%, respectively. On the basis of these findings, the as-synthesized Fe-Al-Mn nanocomposite was successfully applied as a solid phase extraction for preconcentration and determination of Pb(II), Cd(II) and U(VI) ions in aqueous solution.

## 1 Introduction

Heavy metals and radionuclides contamination can cause a significant environmental problem as they are non-degradable and thus persistent [1]. Thus

accurate determination of heavy metals and radionuclides has become increasingly necessary to study problems associated to environmental water pollution. Contamination by heavy metals and radionuclides such as lead, cadmium and uranium to

Address correspondence to E-mail: ayalewame@gmail.com

the surface of water and sediments is due to both natural and anthropogenic activities [2].

The high toxicity of soluble compounds of uranium ( $\text{UF}_6$ ,  $\text{UO}_2(\text{NO}_3)_2$ ,  $\text{UO}_2\text{Cl}_2$ ,  $\text{UO}_2\text{F}_2$ , uranyl-acetate, sulphates and carbonates) is largely manifested in kidney damage [3]. Cadmium and lead are also the most hazardous heavy metals causing great health problems to humans and animal life through accumulation in several organs [4]. Lead is typically poisonous which accumulates in the body and cause kidney malfunctioning, hematological and brain damage [4]. The international agency for research on cancer classified cadmium as a human carcinogen [5]. Therefore, efficient, applicable and affordable techniques are necessary to mitigate the health risk by eliminating or reducing the content of heavy metals and radionuclides from aqueous solution.

Accurate and precise analysis of trace amount of heavy metals by ICP-MS, ICP-AES, and FAAS is an important part of analytical chemistry [6]. Flame atomic absorption spectrometry (FAAS) is among the most widely used methods for the determination of heavy metals ions at trace levels, but its sensitivity is insufficient for the determination in the complex matrix of the environmental sample [7]. Therefore, preconcentration or separation of trace elements from matrices is necessary to improve their detection and sensitivity by FAAS [8]. Solid phase extraction has risen to the forefront methods for the removal of heavy metals due to minimal solvent consumption, flexibility, absence of emulsion [9], high concentration factor and ease of solidification [10]. Thus, SPE based on the distribution of analyte between solution and sorbent is the best method for separation of heavy metals.

Among solid phase adsorbents, silica gel ( $\text{SiO}_2$ ) is widely used due to its mechanical stability at high pressure and low solubility in different solvent. However, silica gel adsorbent exhibited low adsorption capacity and low chemical stability in high acidic and basic media [11]. To improve the performance of solid phase extraction towards metal ions, this material is modified by chelating agent such as Octadecacyclica and amberlite [12]. However, these materials present low reusability as a result of loss of chelating agent after several preconcentration/elution cycles. Fe-Al-Mn nanocomposite is classified as promising ones for heavy metals removals from aqueous solution. This is partly because of their large surface area high activities, high resistance to acids

and bases, high adsorption capacity and low temperature modification [13].

There are plenty of synthesis methods for preparation of nanocomposite such as coprecipitation, sol-gel and hydrothermal [14, 15]. Impregnation methods was used to synthesize Fe-Al-Mn nanocomposite due to its advantages such as good homogeneity, low reaction temperature, uniform particle size, low cost and time saving process [15].

## 2 Methodology

### 2.1 Reagents and solutions

All reagents were analytical grades unless otherwise stated.  $\text{Fe}(\text{NO}_3)_3 \cdot 9\text{H}_2\text{O}$  (98%, BDH, chemicals Ltd, England);  $\text{Al}(\text{NO}_3)_3 \cdot 9\text{H}_2\text{O}$  (98%, Merck, Germany) and  $\text{MnO}_2$  (S. Aldrich) were used as a precursor to prepare Fe-Al-Mn nanocomposite. The standard solution of nitrate salts of Cd(II), Pb(II) and U(IV) (all from Merck) were prepared by diluting a single element stock solution (1000 ppm) with double distilled water.

### 2.2 Synthesis of Fe-Al-Mn nanocomposite

Fe-Al-Mn nanocomposite was synthesized via impregnation method [16]. In a typical synthesis, solution of  $\text{Fe}(\text{NO}_3)_3 \cdot 9\text{H}_2\text{O}$  and  $\text{Al}(\text{NO}_3)_3 \cdot 9\text{H}_2\text{O}$  was prepared separately and mixed together in 70:25 and 60:30 ratios, then 5% and 10%  $\text{MnO}_2$  powder was impregnated in the prepared solution. The product was dried at 150 °C in an oven for 24 h and further calcined at 400, 600 and 700 °C. Finally, the dried materials were ground manually to fine powder using agate mortar for further analysis.

### 2.3 Characterization techniques

The crystal size of as-synthesized Fe-Al-Mn nanocomposite was determined by X-ray diffraction (XRD). The sample was crushed to fine particles and analyzed by X-ray diffractometer, equipped with Cu  $K\alpha$  radiation ( $\lambda = 0.15405 \text{ nm}$ ) at room temperature in the scan range  $2\theta$  between 10 and 90°. The FTIR spectra ( $4000\text{--}400 \text{ cm}^{-1}$ ) were recorded on Parkin Elmer, spectrum 100, FTIR Spectrometer. UV-Vis spectrometer was used to determine the concentration of U (VI) ions whereas the concentration of Cd(II)

and Pb(II) ions was determined by Flame Atomic Absorption spectrometry (FAAS).

## 2.4 Column preparation and preconcentration procedure

The glass column (150 mm length and 8 mm internal diameter) having a stopcock at the bottom and a tank of 250 ml on the top of the column was used. Small amount of glass wool was placed over the stopcock to hold the sorbent. 0.5 g of adsorbent was made slurry in water and placed into the column. Then another small amount of glass wool was inserted onto the top of the sorbent to avoid disturbance of adsorbent during the sample passage. The column was pre-conditioned by passing blank solution having the same pH with the sample solution prior to use. After each use, the nanocomposite was washed with HCl and distilled water respectively and prepared for the second use.

For preconcentration/extraction procedure 50 ml of the pH adjusted sample solution containing  $3 \text{ mg l}^{-1}$  U(VI),  $0.5 \text{ mg l}^{-1}$  Cd(II) and  $5 \text{ mg l}^{-1}$  Pb(II) was taken and allowed to pass through the packed column at a flow rate of  $5 \text{ mg min}^{-1}$  [17]. The retained analyte was eluted with 10 ml of 0.5 M of HCl and determined by FAAS. Uranium is separately determined by UV-Vis spectroscopy using EDTA indicator solution at  $\lambda_{\text{max}}$  557 nm. The effect of pH was studied in the pH range of 2–10 keeping the other parameters constant.

## 3 Results and discussion

### 3.1 XRD analysis

In order to characterize nature and crystal size of nanocomposite, X-ray diffraction pattern was investigated. According to the result, the patterns at  $2\theta$  value of 24, 34, 36, 42, 49.5, 55, and 64.5 corresponds to hematite and the remaining weak peaks at  $2\theta$  value of 57.5 and 63.5 corresponds to bauxite (Fig. 1) [15, 18, 19]. This may be due to the small percentages of  $\text{MnO}_2$  dominated by  $\text{Fe}_2\text{O}_3$  and  $\text{Al}_2\text{O}_3$ . The crystal size was estimated from the basic Scherrer equation [18].  $D = \frac{k\lambda}{\beta \cos\theta}$  Where  $D$  is the average crystallite size,  $\lambda$  is the X-ray wavelength,  $\beta$  is the width of the X-ray peak on  $2\theta$  axis, normally measured as full width at half maximum (FWHM),  $\theta$  is

bragg angle, and  $k$  is Scherrer constant.  $K$  depends on the crystallite shape and the size distribution, indices of the diffraction line, and the actual definition used for  $\beta$  whether FWHM or integral breadth [20].  $K$  can have values anywhere from 0.62 and 2.08. In this paper,  $K = 0.9$  was used.

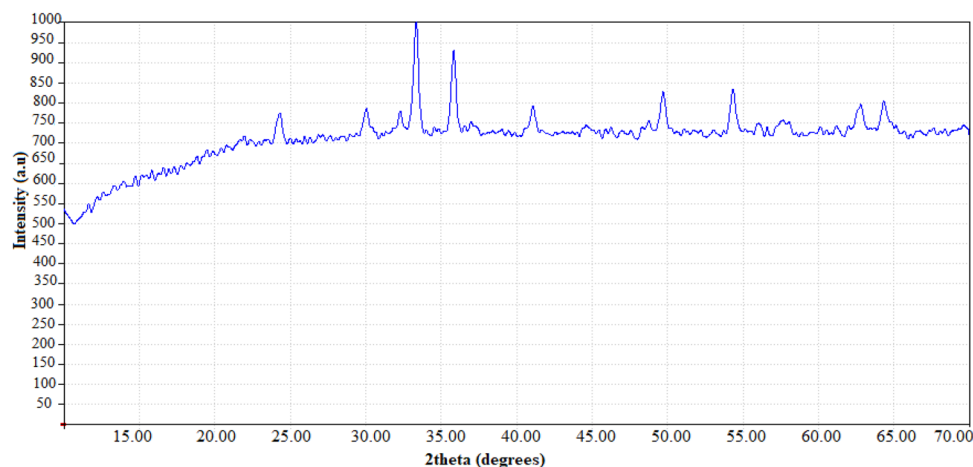
According to the result, the average crystalline size of the nanocomposites varied between 30.81–35.15 nm. The sample with large crystal size (34.98 nm) and small ratio of  $\text{Al}_2\text{O}_3$  (Table 1) was selected for further adsorption studies. This large crystal structure of nanosorbent was selected due to large abrasion resistance and uniformity, while small ratio of  $\text{Al}_2\text{O}_3$  was selected because large alumina content delays crystallite of nanocomposite.

The calcination temperature has important rule to play information of the crystalline phase and the particle size. The particle sizes of two samples calcined at three different temperatures (400, 600 and 700 °C) are compared (Table 1). It was observed that the crystal size of the nanocomposite increased when the calcination temperature increases.

The adsorbent materials with different ratios Fe: Al: Mn (70:25:5 and 60:30:10) was investigated. From the result, it is noted that increasing the alumina content delay crystallization [21]; however, the concomitant increase in manganese oxide could have counter effect which might have led to increase crystal size as the temperature increases. On the other hand, the presence of large amount of manganese dioxide powder delays the uniformity of nanocomposite [22]. Therefore Fe-Al-Mn ternary mixed oxides that contains small percentage of manganese dioxide was used for adsorption of metal ions.

### 3.2 SEM-EDX analysis

Scanning electron microscopy coupled with energy dispersive X-ray detector (SEM-EDX) was used to observe the morphology particle size and composition of Fe-Al-Mn nanocomposite. SEM corroborate (Fig. 2a) the presence of homogenous particle size with crystal size 10  $\mu\text{m}$ . The energy dispersive X-ray detector image (Fig. 2b) shows a relative percentage by mass of Fe, Al and Mn were 51.32, 5.34 and 1.63%, respectively.

**Fig. 1** XRD pattern of as-synthesized nanocomposite**Table 1** Crystal sizes (D) of as-synthesized nanocomposite

Sample code	2θ (degree)	β (degree)	D (nm)
1 (400 °C)	33.960	0.283	30.81
2 (400 °C)	33.980	0.254	30.70
1 (600 °C)	33.780	0.257	33.75
2 (600 °C)	33.800	0.245	34.08
1 (700 °C)	33.960	0.248	34.98
2 (700 °C)	33.960	0.247	35.15

### 3.3 Infrared spectroscopic studies

FTIR spectra of as-synthesized nanocomposite before and after adsorption of metal ions are shown in Fig. 3. Absorption peak at  $867\text{ cm}^{-1}$  corresponds to the symmetric stretching of Al-O bond and the peak around  $1025\text{ cm}^{-1}$  corresponds to the Fe-O stretching of  $\text{Fe}_2\text{O}_3$  phase [23]. Absorption band around  $3461\text{ cm}^{-1}$  corresponds to OH stretching frequency of  $\text{AlO}(\text{OH})$  phase [11]. A peak observed at  $1639\text{ cm}^{-1}$  was attributed to the bending vibration of hydroxyl group of iron hydroxides (Fe-OH) [24]. Absorption peak centered at  $536\text{ cm}^{-1}$  shows the presence of hematite and the band spectrum at 462 and  $536\text{ cm}^{-1}$  indicates the presence of metal oxide bond vibration. The intensity of the peaks after adsorption were relatively higher than before adsorption, due to the availability of more  $\text{H}_2\text{O}$  in aqueous media and is assigned to the deformation of water molecules and the presence of adsorbed water and hydroxyl groups on the metal oxide surface. After adsorption, new peak appears at  $994\text{ cm}^{-1}$  which is binding vibration of adsorbed metals and the peak at  $1448\text{ cm}^{-1}$  corresponds to adsorbed water of metal oxide [25]. This

indicates that there were adsorbed metal ions on the adsorbent surface.

### 3.4 Effect of pH of sample solution

pH in one of the most important environmental factors influencing not only the site of adsorbent but also the solution chemistry of heavy metals [26]. According to the result (Fig. 4), the recovery of Pb(II), Cd(II) and U(IV) ions were quantitative  $\geq 95\%$ , at pH value of 6, 7 and 4, respectively. At higher pH value, the adsorption of these metal ions declined due to the precipitation of Pb(II), Cd(II) and U(IV) ions forming  $\text{Pb}(\text{OH})_2$ ,  $\text{Cd}(\text{OH})_2$  and  $\text{UO}_2(\text{OH})$  on the surface of the sorbent. This precipitate blocks the pores of the nanosorbent which led to a decrease of adsorption capacity. On the other hand, at lower pH value, the  $\text{H}_3\text{O}^+$  compete with the metal ions for the exchange site in the adsorbent and restrict the approach of metal cations as a result of the repulsion force [27].

### 3.5 Effect of amount of Fe-Al-Mn nanocomposite

A quantitative retention of analyte is not obtained when the amount of the sorbent is less whereas, an excess amount of adsorbent prevents the elution of the retained analyte by small volume of eluent [28]. Therefore, the influences of the amount of Fe-Al-Mn nanosorbent on the retention of Pb(II), Cd(II) and U(IV) ions were examined. According to the result, the recovery of Cd(II), Pb(II) and U(IV) ions increased with increasing amounts of Fe-Al-Mn nanosorbent and reached a maximum value of over 95% at 500 mg (Fig. 5). Above 500 mg of Fe-Al-Mn nanosorbent, the



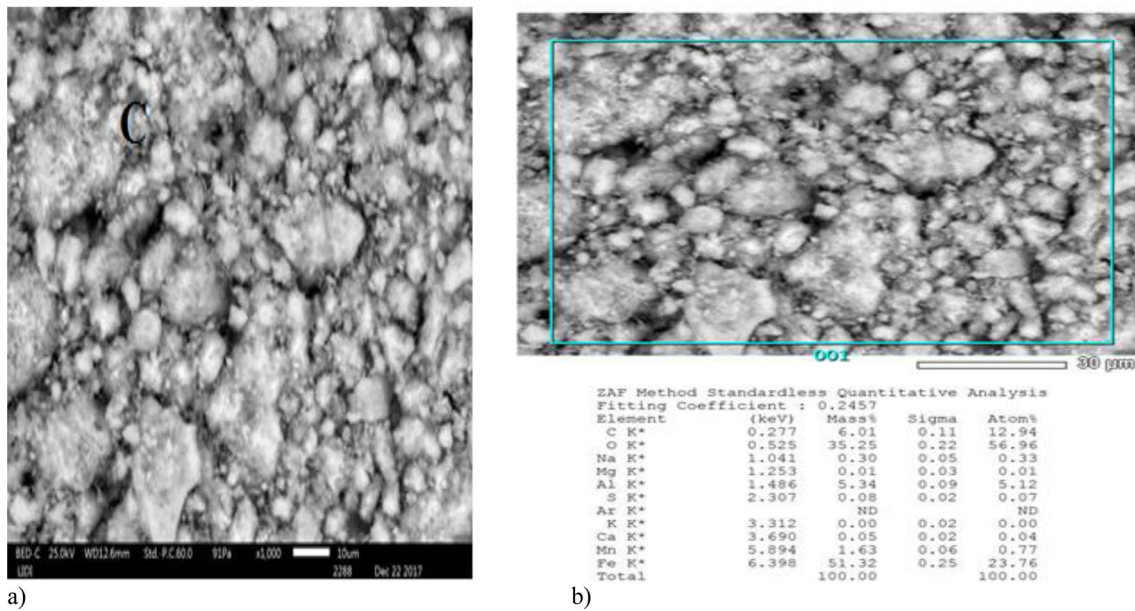
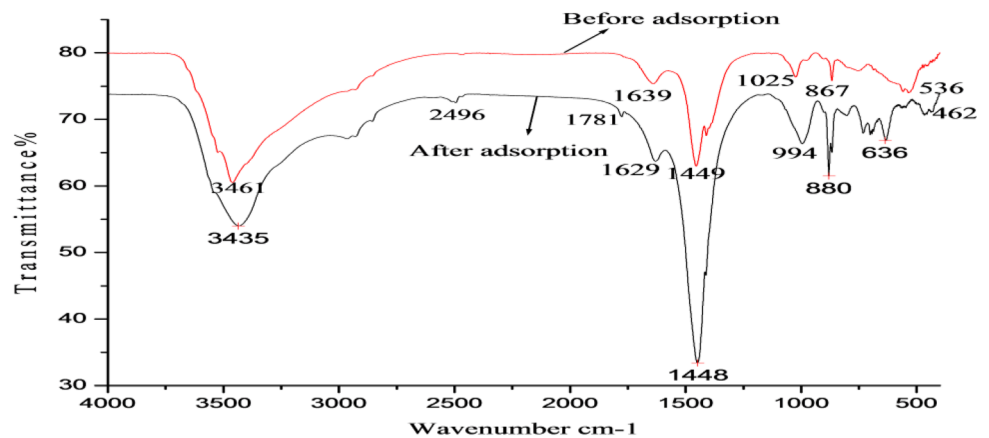


**Fig. 2** a Scanning electron microscopy and b energy dispersive X-ray detector image of Fe–Al–Mn nanocomposite

**Fig. 3** FTIR spectrum of Fe–Al–Mn nanocomposite before and adsorption study



recoveries of Cd(II), Pb(II) & U(IV) ions decreased because the retained metal ions cannot be eluted completely with 10 ml of 0.5 M HCl solution. On the other hand, when the amount of sorbent was below 300 mg, quantitative recovery of Cd(II), Pb(II) and U(IV) ions were not obtained because at low adsorbent dose, enough active sites are not available. Therefore, 500 mg of adsorbent was used for subsequent experiment.

### 3.6 Effect of type, concentration and volume of the eluent

A suitable and efficient eluent must be used for elution of adsorbed metal ions on Fe–Al–Mn nanocomposite with small volume to obtain a high enrichment

factor and avoid influence the life and reusability of adsorbent. In lower pH, the metal–ligand complex dissociates to release metal ions. Therefore, acidic eluent is the best choice to obtain efficient extraction [29].

For the elution process HNO<sub>3</sub> and HCl having various concentrations and volume were tested to obtain quantitative recovery of Cd(II), Pb(II) and U(IV) ions from the nanosorbent packed in the column. According to the result in Table 2, HCl solutions that give maximum recovery in range of 97–98.5 were found as optimum eluents. Results show the recovery was increased as the concentration of HCl increased up to 0.5 M and beyond which the recovery declined. The use of low concentration of HCl is beneficial because it can increase the life time of the

**Fig. 4** Recovery of Cd(II), Pb(II) and U(IV) ions as a function of pH (eluent: 15 ml of 0.5 M HCl, amount of adsorbent: 500 mg,  $n = 3$ )

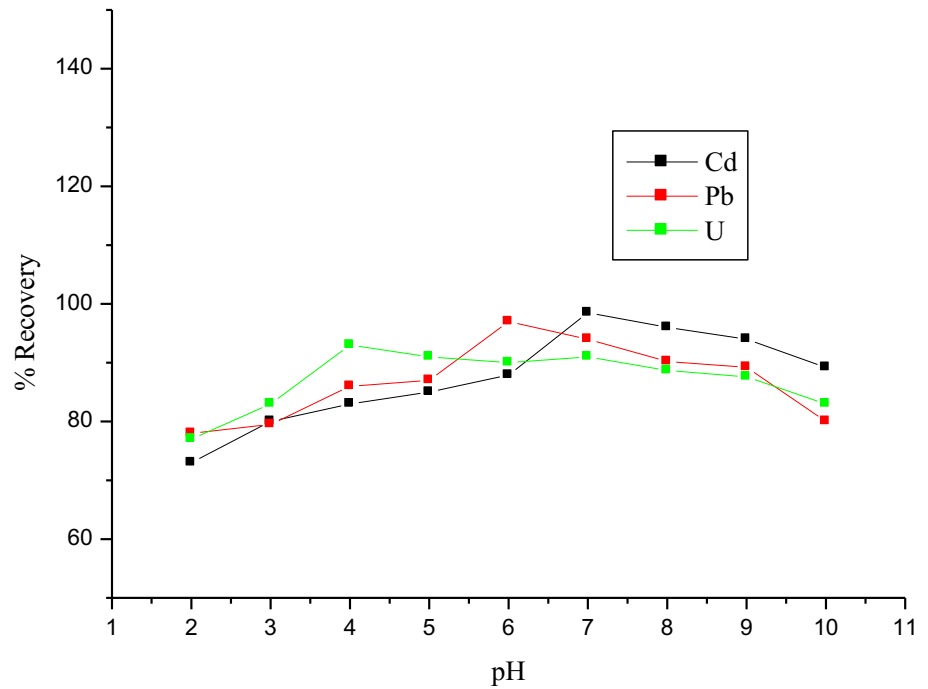


**Fig. 5** Effect of amount of Fe–Al–Mn nanocomposite on the extraction recovery of Pb(II) (eluent; 15 ml of 0.5 M HCl, pH 7, 6 and 4, respectively,  $n = 3$ )

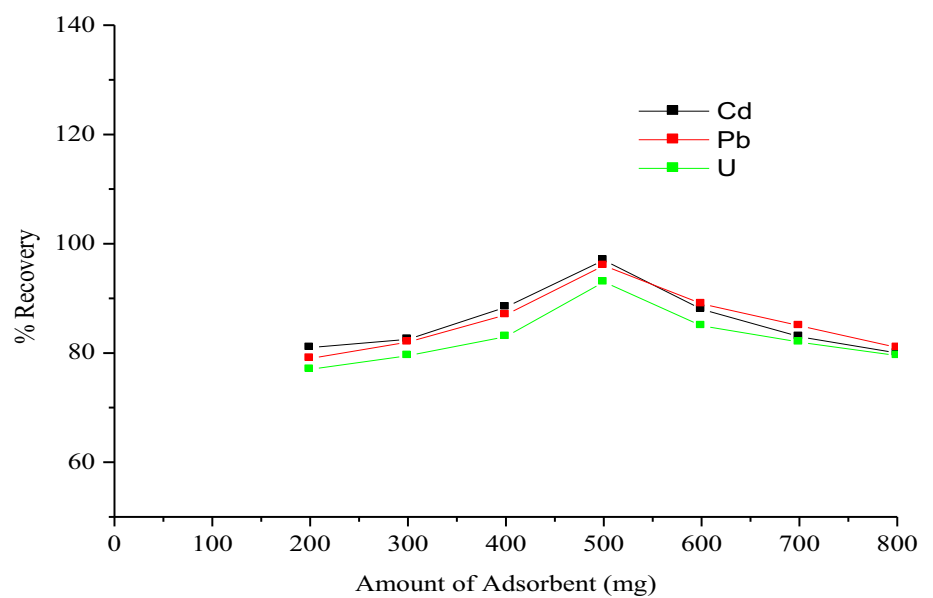


**Table 2** Effect of type, concentration and volume of the eluent

Eluent type		HCl 0.1 M	HCl 0.5 M	HCl 1 M	HCl 2 M	HNO <sub>3</sub> 0.1 W	HNO <sub>3</sub> 0.5 M	HNO <sub>3</sub> 1 M	HNO <sub>3</sub> 2 M
Recovery (%)	Cd(II)	91	97.5	93.5	88	80	95	91	89.5
	Pb(II)	93.4	98	94	87.6	78	97	87.6	85.4
	U(VI)	76.9	98.5	87.6	81.5	90	95	93.3	81

column; whereas high concentration decreases the lifetime of the column by dissolving the adsorbent. Therefore, 0.5 M of HCl was chosen as the eluent owing to effective elution of adsorbed Cd(II), Pb(II) and U(VI) ions from aqueous solution (Table 2).

Various volumes of 0.5 M HCl were also examined as eluent for desorbing the retained analytes from the solid phase. Since quantitative recovery ( $\geq 95\%$ ) was obtained with 10 ml of 0.5 M HCl solution, it was selected as an eluent (Fig. 6).

### 3.7 Effect of flow rate of sample solution

The flow rate of sample solution through the column was not only affecting the recovery of analyte but also control the time of analysis. According to the result the percentage recovery decreases with increasing flow rate, which is due to the shorter contact time between the adsorbent and sample solution (Fig. 7). Therefore, a flow rate of 5 ml/min was chosen to compromise between analytical time and the quantitative recovery of analyte.

### 3.8 Effect of sample volume

In order to obtain higher enrichment factor large volume of sample solution is required. According to the result in Fig. 8, quantitative recovery was obtained with sample volume of up to 150 ml. The recoveries of ions decrease with increasing sample volume due to the excess analytes loaded over the

column capacity. As a result, it can be concluded that  $0.067 \text{ mgL}^{-1}$  of Cd(II), Pb(II) and U(VI) ions could be determined with a sample volume of 150 ml.

### 3.9 Reusability of the sorbent

The stability and reusability of the sorbent were assessed by monitoring the variation in the recovery of analyte through several adsorption elution cycles. The reusability of the present matrix was examined with the passage of 50 ml sample containing  $2 \text{ mg l}^{-1}$  analyte solutions, 10 ml of 0.5 M HCl eluent and 15 ml of deionized water respectively through the column packed with 500 mg of nanocomposite.

Adsorption capacity is slightly decreasing continuously as the number of cycle increase Fig. 9. This is because precipitate formed during adsorption blocks the pores of the nanocomposite which led to a decrease of its adsorption capacity. However, the trace heavy metal ions in a sample solution can be quantitatively retained after seven repeated uses and the mean recovery for the metal ions were found to be in the range of 95.0–99.9%. This clearly shows that the column could be reused up to seven times with quantitative recovery.

### 3.10 Effect of interfering ions

One of the most important targets of preconcentration procedures is elimination of interfering ions from the sample. The reliability of the method has to

**Fig. 6** Effect of the volume of 0.5 M HCl solution on the recovery of Cd(II), Pb(II) and U(VI) ions by Fe–Al–Mn nanosorbent ( $n = 3$ )

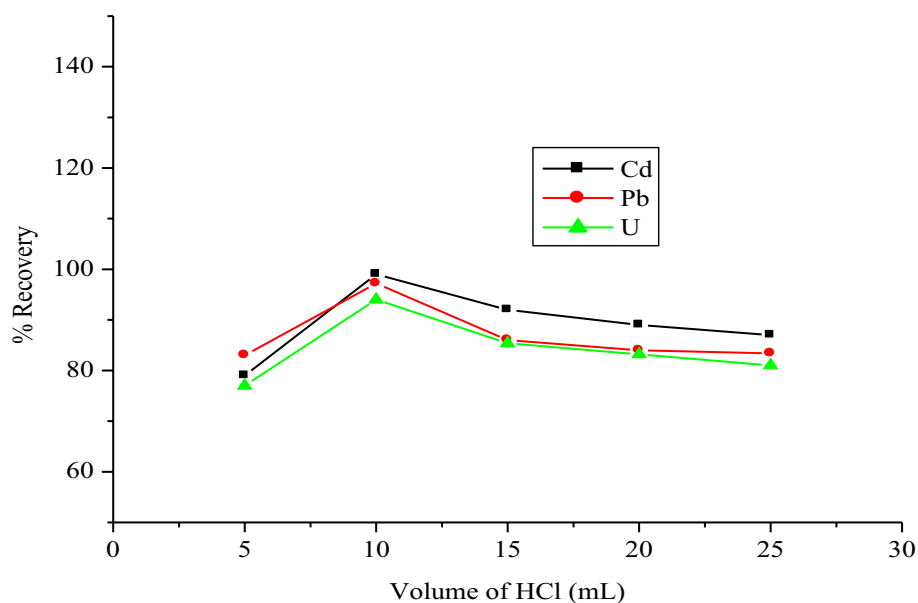


**Fig. 7** plot of % recovery Cd(II), Pb(II) and U(VI) ions as a function of eluent(0.5 mol l<sup>-1</sup> HCl) flow rate of sample solution (*n* = 3, V = 50 ml, adsorbent dose = 500 mg

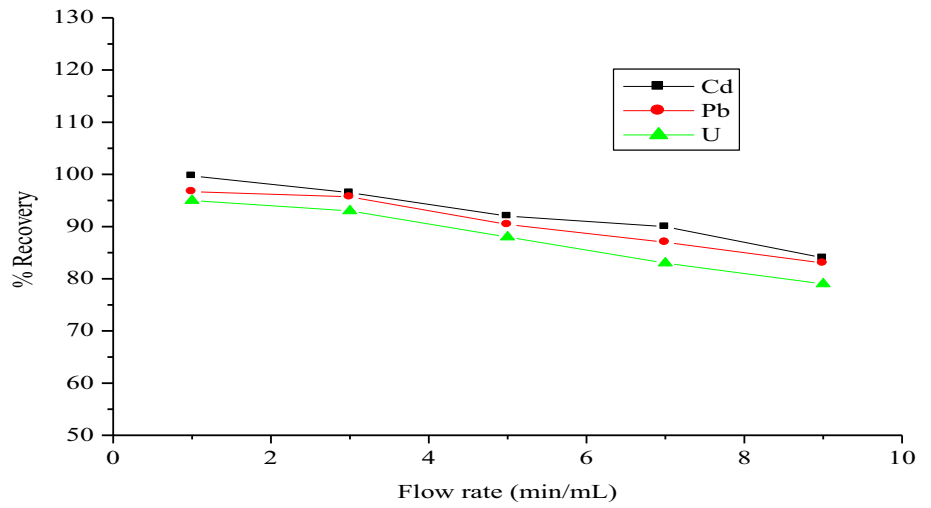


**Fig. 8** Plot of % recovery of U(VI), Pb(II) and Cd(II) ions by Fe–Al–Mn nanosorbent as a function of sample volume (eluent; (10 ml of 0.5 M HCl) *n* = 3)

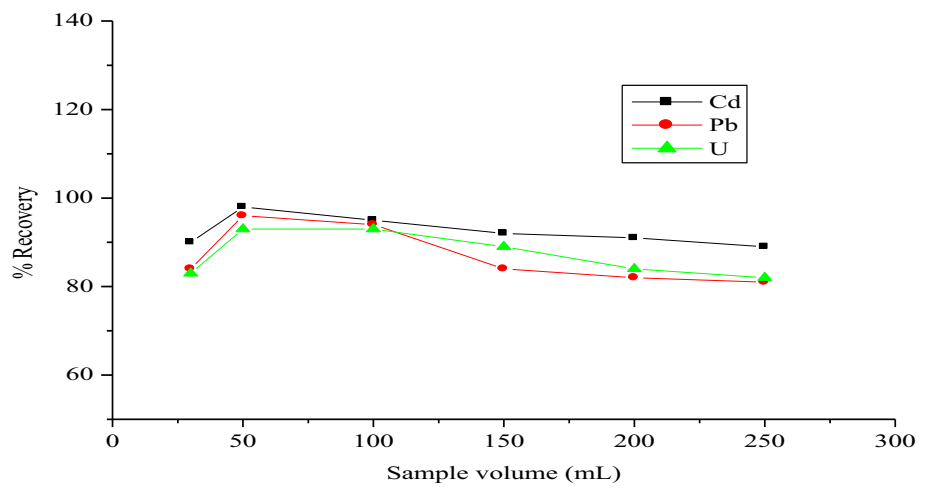


**Fig. 9** Plot of % recovery of U(VI), Pb(II) and Cd(II) ions vs number of cycle (eluent; (10 ml of 0.5 M HCl) *n* = 3)

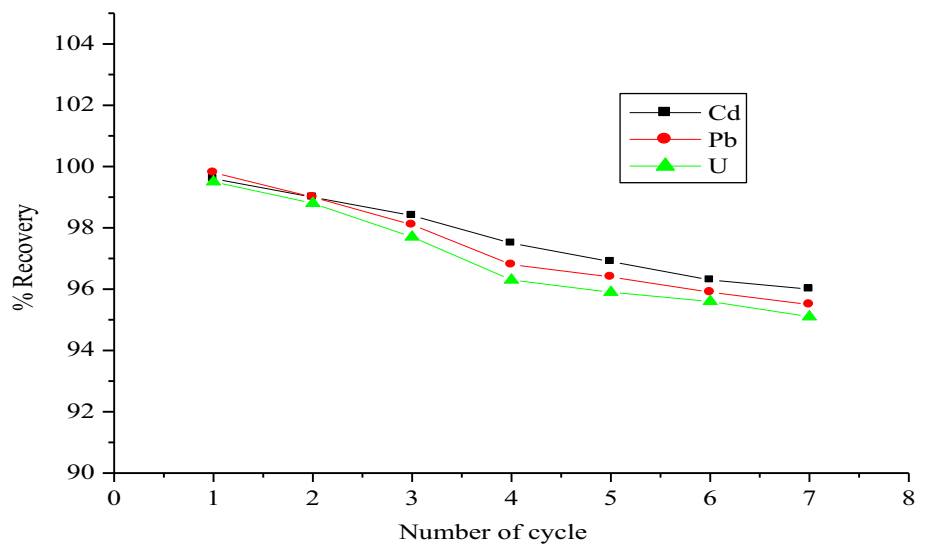




**Table 3** Effect of the interference ions

Interfering ions	Conc.(mg l <sup>-1</sup> )	Recovery (%)		
		Cd(II)	Pb(II)	U(VI)
Cr(III)	25	97.6 ± 1.0	99 ± 1.2	87.3 ± 1.5
	35	96.7 ± 2.0	98 ± 3.0	82.3 ± 2.0
	50	92.2 ± 2.5	95 ± 1.4	81.7 ± 2.1
Co(II)	15	98.2 ± 2	98.2 ± 1.2	85.7 ± 1.5
	3525	96.1 ± 1	96.7 ± 2.0	84.9 ± 3.5
	50	91.5 ± 2	96.0 ± 2.1	81.0 ± 1.1
Cu(II)	20	94.5 ± 2	96.7 ± 3	84.2 ± 2.3
	35	92.0 ± 2	96.0 ± 1	81.6 ± 2.0
	50	93.3 ± 3	96.8 ± 2	81.3 ± 3.0
Zn(II)	15	97.7 ± 2	97.8 ± 2	88.8 ± 2.8
	25	97.3 ± 2	96.6 ± 3	83.0 ± 1.0
	40	97.8 ± 1	97.0 ± 1	81.0 ± 3.0
Ni(II)	15	93.0 ± 1	97.5 ± 2.0	81.3 ± 1.5
	25	91.8 ± 1	95.8 ± 2.5	80.3 ± 2.1
	40	91.1 ± 2	93.0 ± 4.0	77.9 ± 2.2

**Table 4** Langmuir and freundlich constant for the sorption of Cd(II), U(VI) and Pd(II), ions

Analytes	Langmuir model				Freundlich model		
	Q <sub>o</sub> (mg/g)	b	R <sub>L</sub>	R <sup>2</sup>	K <sub>f</sub>	1/n	R <sup>2</sup>
Pb(II)	12.5	1.000	0.050	0.997	1.2	0.297	0.957
Cd(II)	12.8	0.769	0.060	0.995	5.25	0.317	0.951
U(VI)	14.9	1.046	0.046	0.991	6.516	0.372	0.977

be examined in the presence of possible interference ions which affect the adsorption of target analyte. As can be seen from Table 3, the recovery for Pb(II) and Cd(II) ions were quantitative (> 90%) in the presence of studied interference ions. However, the interfering ions present in water sample form stable complex with EDTA when determined with UV-visible spectroscopy, as the result, a slightly decreased recovery of U(VI) ion was noted. However, U(VI) ion was quantitatively retained on Fe-Al-Mn nanosorbent. These results indicate that the developed preconcentration method for Pb(II) and Cd(II) ions was not affected by the presence of interference, which also applied to highly saline samples that contains some transitional metals in mg l<sup>-1</sup> level.

### 3.11 Adsorption isotherm

The adsorption isotherm was used to characterize interaction of each analyte with adsorbent. The most widely accepted surface adsorption models are Langmuir and Freundlich models. Langmuir

adsorption isotherm which is valid for monolayer adsorption onto a surface with finite number of identical sites and based on the assumption of surface homogeneity such as equally available adsorption site and no interaction between adsorbed species [30]. The Freundlich adsorption isotherm model is an empirical relationship describing the adsorption of solute; it assumes different site with different adsorption energies [31].

The linearized Langmuir and Freundlich plots for Pb(II), Cd(II) and U(VI) are given in Fig. 9 (a), (b), and (c), respectively. The slope and intercept of the linearized Langmuir and Freundlich plots were used to calculate the adsorption constant tabulated on Table 4. The higher correlation coefficients of Langmuir adsorption isotherm indicate that this model fits the adsorption data better than the Freundlich model. For Langmuir adsorption isotherm, the essential characteristics can be expressed in terms of a dimensionless parameter ( $R_L = 1/1 + bC_0$ ). The value of  $R_L$  indicates the type of the isotherm to be unfavorable, linear or favorable.  $R_L$  value for all

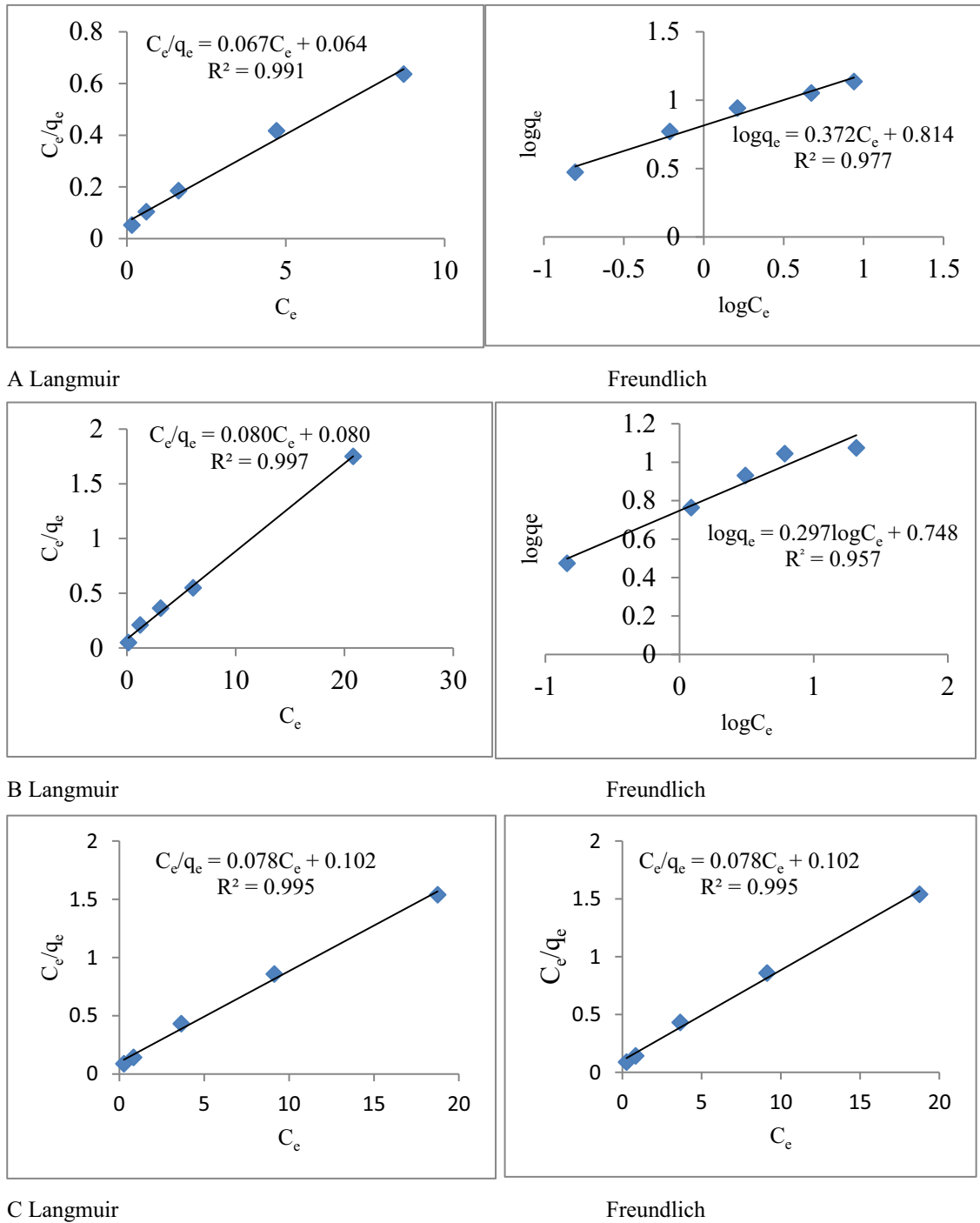


**Fig. 10** Linearized Langmuir and Freundlich adsorption isotherm of **A** U(VI), **B** Pd(II) and **C** Cd(II) ions on Fe-Al-Mn nanocomposite, respectively

concentration is in between 0 and 1 indicating favorable adsorption (Table 4).

From the plot of  $\log q_e$  versus  $\log C_e$ , Fig. 10 yields a straight line. The value of  $1/n$  lying between 0 and 1 (0.372, 0.297 and 0.317), for U(VI), Pb(II), and Cd(II) respectively indicate a favorable condition for

adsorption and the physical adsorption of metal ions onto Fe-Al-Mn nanocomposite [32]. From the plot of  $C_e/q_e$  versus  $C_e$ , (Fig. 10), the maximum adsorption capacity of Fe-Al-Mn nanocomposite for Cd(II), U(VI) and Pd(II), ions were found 12.8, 14.9 and 12.5 mg/g, respectively. Therefore, for the sorption isotherm of

**Table 5** Results for method detection limits for tap water samples and lake water samples

Metal ions	RSD%	IDL (mg/L) <sup>a</sup>	MDL for tap water(mg/L) <sup>b</sup>	MDL for lake water(mg/L) <sup>b</sup>
Pb(II)	2.47	0.080	0.090	0.080
Cd(II)	0.98	0.010	0.050	0.060
U(II)	2.04	0.003	0.0097	0.008

<sup>a</sup>Concentration corresponding to instrument detection limit<sup>b</sup>Concentration corresponding to ten standard deviations of the blank

MDL Method detection Limit, IDL Instrumental Detection Limits

**Table 6** Results for the determination of Pb(II), U(VI) and Cd(II) ions using the proposed procedure

Sample	Cd(mg L <sup>-1</sup> )		R%	Pb(mg L <sup>-1</sup> )		R%	U(mg L <sup>-1</sup> )		R%
	added	Found		Added	found		Added	found	
Tap water	0	1.61 ± 0.07	86.6	0	3.31 ± 0.09	92.77	0	1.55 ± 0.20	81.8
	2	3.25 ± 0.13		4	6.33 ± 0.10		1	2.84 ± 0.12	
Lake water	0	0.73 ± 0.04	91.3	0	3.72 ± 0.04	93.6	0	0.21 ± 0.21	81.0
	3	3.59 ± 0.13		5	8.21 ± 0.15		1	1.42 ± 0.13	

R: recovery, *n* = 3

Cd(II), U(VI) and Pd(II), ions Langmuir equation was fitted more to the experimental data compare to Freundlich. But both Freundlich and Langmuir equation were fitted to the experimental data satisfactorily. According to the result the maximum capacity of adsorbent in column condition, due to the less duration of contact time is slightly less than the batch system, which is apparently quite expected [33].

### 3.12 Analytical method detection limit

The limits of detection for studied elements based on three standard deviations (*n* = 10) of the blank signal are summarized in Table 5. The method detection limit is generally comparable with that of instrument for both tap water and lake water samples. The concentration of Cd(II), U(VI) & Pb(II) ions determined in the tap water samples, were higher than the procedure detection limit.

Similarly, the concentration of Cd(II) and Pb(II) ions determined in the lake water samples are 91.8 and 97.8 times higher than the corresponding procedure detection limits, thus giving rise to good precision. The detection limit of the proposed method was comparable to those obtained by other methods described in the literature [34]. The relative standard deviation (*n* = 10) was < 2.5% for Cd(II), U(VI) and

Pb(II) ions indicating that this method is highly precise and reproducible (Table 5).

### 3.13 Recovery studies in tap and lake water samples

The validity of the proposed method was tested by spiking known concentrations of Cd(II), U(VI) and Pb(II) to tap water (taken from Haramaya University), and lake water (taken from Adele) samples. The water samples were filtered and stored in polythene bottles. From the result indicated in Table 6, the concentration of Pb(II), U(VI) and Cd(II) ions for tap water were found to be 3.31, 1.55 and 1.61 mg l<sup>-1</sup>, respectively. The concentration of Pb(II), U(VI) and Cd(II) ions for lake water sample was 3.7, 0.73 and 0.2 mg l<sup>-1</sup>, respectively. The percentage recovery of U(VI) ion in lake water sample is lower as compared with Pb(II) and Cd(II) ions (Table 6). These results indicated that the developed preconcentration method for Cd(II) and Pb(II) was not affected by the potential interferences from the major matrix components of the water sample. But, since the interferences present in lake water sample such as Cr(III), Co(II), Cu(II) and Zn(II) ions form stable complex with EDTA when measured with Uv-visible spectroscopy, the recovery of U(VI) ions was less. This can be improved using arsenazo (III) which form stable complex with U(VI) [35]. Nonetheless, U(VI)

**Table 7** Comparative data for various SPE preconcentration methods

Analyte	Preconcentration system	LOD (mgL <sup>-1</sup> )	Adsorption Capacity (mg g <sup>-1</sup> )	PF	Determination technique	Ref
V, Cr, Mn, Ni, Cu, Zn, Cd, Pb	Nanometer-sized alumina	$6 \times 10^{-6}$ – $79 \times 10^{-6}$	1–18	5	ICP-MS	[36]
Cr, Cu, Pb	Magnetic nanoparticle/Bismuthiol II	$4.3 \times 10^{-5}$ – $8.5 \times 10^{-5}$	5.4–9.4	87–96	FAAS	[37]
U	Diaryiazobisphenol Modified activated carbon	$3.8 \times 10^{-2}$	18.35	–	Uv-visible	[3]
Cu, Co Cd	Nano ZrO <sub>2</sub> /B <sub>2</sub> O <sub>3</sub>	$3.1 \times 10^{-3}$ – $3.8 \times 10^{-3}$	32.2–109.9	10–15	FAAS	[38]
Cd, Pb, U	Nano Fe–Al–Mn	$3 \times 10^{-3}$ – $8 \times 10^{-3}$	12.5–14.9	5–15	FAAS and Uv-visible	This work

PF preconcentration factor, ICP-MS Inductively Plasma Mass Spectroscopy, FAAS Flame Atomic Absorption Spectroscopy

ion was quantitatively retained on Fe–Al–Mn nanosorbent.

### 3.14 Comparison of the method with others

The analytical performance of the nanosorbent was comparable with the other conventional sorbents. Some comparative data about sorption are summarized in Table 7. Limit of detection, adsorption capacity and preconcentration factors obtained are comparable to those presented by other methods. The present work

evidenced relatively high adsorption capacity when compared with reported methods [37, 38]. On the other hand, limit of detection was similar to those reported by previous methods [38], preconcentration factor is relatively higher than those of the others methods [36].

## 4 Conclusion

Fe–Al–Mn nanocomposite as a new solid phase extractor provides a simple, selective, accurate, economical, rapid and precise method for preconcentration and determination of Pb(II), U(VI) and Cd(II) ions from aqueous solution. There is no need to use any complexing or chelating agent for modifying the sorbent to obtain quantitative recovery of Pb(II), U(VI) and Cd(II) ions. The preconcentration procedure described in this paper allows Pb(II), U(VI) and Cd(II) ions determination at low concentration level in various water samples, whose analysis would be restricted due to poor sensitivity of flame atomic adsorption spectrometry. The selectivity was excellent making it possible to detect and determine Pb(II), U(VI) and Cd(II) ions in the presence of high concentration of foreign ions. The limit of detection based on three times the standard deviation of the blank was reported to be 0.09, 0.05 and 0.0097 mg g<sup>-1</sup> for Pb(II), Cd(II) and U(VI) ions, respectively. In addition, this method is sensitive, low cost and doesn't need sophisticated instruments such as ICP-OES or GF-AAS.

## Acknowledgements

Authors are thankful to PGDP (the then SGS) of Haramaya University and Department of Chemistry for the financial support.

## Author contributions

The first Author conducts all laboratory works, collects and analyze the data and wrote the manuscript. The contribution of other authors (co-author) was, conceptualizing, supervising, and reviewing the manuscript.

## Funding

The authors have not disclosed any funding.

## Data availability

The data supporting the finding of this study are available from the corresponding author on reasonable request.

## Declarations

**Conflict of interest** The authors declare that there is no conflict of interest.

## References

1. M.A. Hashem, M.S. Nur-A-Tomal, N.R. Mon-dal, M.A. Rahman, Hair burning and liming in tanneries is a source of pollution by arsenic, lead, zinc, manganese and iron. *Environ. Chem. Lett.* **15**, 501–506 (2017)
2. U. Oeh, N.D. Priest, P. Roth, K.V. Ragnarsdottir, W.B. Li, V. Höllriegl, M.F. Thirlwall, B. Michalke, A. Giussani, P. Schramel, H.G. Paretzke, Measurements of daily urinary uranium excretion in German peacekeeping personnel and residents of the Kosovo region to assess potential intakes of depleted uranium (DU). *Sci. Total Environ.* **381**(1–3), 77–87 (2007)
3. M. Kapnisti, F. Noli, P. Misaelides, G. Vourlias, D. Karfaridis, A. Hatzidimitriou, Enhanced sorption capacities for lead and uranium using titanium phosphates; sorption, kinetics, equilibrium studies and mechanism implication. *Chem. Eng. J.* **342**, 184–195 (2018)
4. A. Wilk, E. Kalisińska, D.I. Kosik Bogacka et al., Cadmium, lead and mercury concentrations in pathologically altered human kidneys. *Environ. Geochem. Health.* **39**, 889–899 (2017)
5. Y. Zhai, Y. Liu, X. Chang, S. Chen, X. Huang, Selective solid-phase extraction of trace cadmium (II) with an ionic imprinted polymer prepared from a dual ligand monomer. *Anal. Chim. Acta* **593**, 123–128 (2007)
6. N. Manousi, G.A. Zachariadis, Development and application of an ICP-AES method for the determination of nutrient and toxic elements in savory snack products after autoclave dissolution. *Separations* **7**(4), 66 (2020)
7. A.B.M. Helaluddin, R.S. Khalid, M. Alaama, S.A. Abbas, Main analytical techniques used for elemental analysis in various matrices. *Trop. J. Pharm. Res.* **15**, 427–434 (2016)
8. O.T. Butler, W.R. Cairns, J.M. Cook, C.M. Davidson, R. Mertz-Kraus, Atomic spectrometry update review of advances in environmental analysis. *J. Analyt. At. Spectrom.* **33**, 8–56 (2018)
9. F. Sabermahani, M.A. Taher, H. Bahrami, Separation and preconcentration of trace amounts of gold from water samples prior to determination by flame atomic absorption spectrometry. *Arab. J. Chem.* **9**, S1700–S1705 (2016)
10. Z. Guo, Y. Li, S. Zhang, H. Niu, Z. Chen, J. Xu, Enhanced sorption of radiocobalt from water by Bi (III) modified montmorillonite: a novel adsorbent. *J. Hazard. Mater.* **192**, 168–175 (2011)
11. B. Kırkan, G.A. Aycik, Solid phase extraction using silica gel modified with azo-dyes derivative for preconcentration and separation of Th (IV) ions from aqueous solutions. *J. Radioanal. Nucl. Chem.* **308**(1), 81–91 (2016)
12. R.K. Sharma, P. Pant, Preconcentration and determination of trace metal ions from aqueous samples by newly developed Gallic acid modified Amberlite XAD-16 chelating resin. *J. Hazard. Mater.* **163**(1), 295–301 (2009)
13. J. Yang, B. Hou, J. Wang, B. Tian, J. Bi, N. Wang, X. Li, X. Huang, Nanomaterials for the removal of heavy metals from wastewater. *Nanomaterials* **9**, 424 (2019)
14. L.M. Anaya-Esparza, E. Montalvo-González, N. González-Silva, M.D. Méndez-Robles, R. Romero-Toledo, E.M. Yahia, A. Pérez-Larios, Synthesis and characterization of TiO<sub>2</sub> ZnO MgO mixed oxide and their antibacterial activity. *Materials* **12**, 698 (2019)
15. B. Abebe, A. Tadesse, T. Kebede, E. Teju, I. Diaz, Fe-Al-Mn ternary oxide nanosorbent: synthesis, characterization and phosphate sorption property. *J. Environ. Chem. Eng.* **5**, 1330–1340 (2017)
16. N.B. Wutke, K.M. Diniz, M.Z. Corazza, F.M.D. Oliveira, E.S. Ribeiro, B.T. da Fonseca, M.G. Segatelli, C.R. Teixeira-Tarley, Preconcentration of nickel (II) by a mini-flow system with a novel ternary oxide solid phase and flame atomic absorption spectrometry. *Analyt. Lett.* **49**, 723–736 (2016)
17. L.M. Colletti, R. Copping, K. Garduno, E.J. Lujan, A.K. Mauser, A. Mechler-Hickson, I. May, S.D. Reilly, D. Rios, J. Rowley, A.B. Schroeder, The application of visible absorption spectroscopy to the analysis of uranium in aqueous solutions. *Talanta* **175**, 390–405 (2017)

18. A. Tofik, M.T. Abi, K. Tesfahun, G. Girma, Fe-Al binary oxide nanosorbent: synthesis, characterization and phosphate sorption property. *J. Environ. Chem. Eng.* **4**, 2458–2468 (2016)
19. R.H. Nejat, T.M. Abi, T. Ayalew, Synthesis, characterization and photocatalytic activity of  $\text{MnO}_2/\text{Al}_2\text{O}_3/\text{Fe}_2\text{O}_3$  nanocomposite for degradation of malachite green. *Bull. Chem. Soc. Ethiop.* **32**, 101–109 (2018)
20. A.M.G. Carvalho, D.H.C. Araujo, H.F. Canova, C.B. Rodella, D.H. Barrett, S.L. Cuf-fini, R.N. Costa, R.S. Nunes, X-ray powder diffraction at the XRD1 beamline at LNL. *J. Synchrotron. Rad.* **23**, 1501–1506 (2016)
21. J.D. Li, Y.L. Shi, Y.Q. Cai, S.F. Mou, G.B. Jiang, Adsorption of di-ethyl phthalate from aqueous solutions with surfactant coated nano/microsized alumina. *J. Chem. Eng.* **140**, 214–220 (2008)
22. T. Herranz, S. Rojas, M. Ojeda, F.J. Perez-Alonso, P. Terreros, K. Pirota, L.G. Fierro, Synthesis, structural features, and reactivity of Fe-Mn mixed oxides prepared by microemulsion. *Chem. Mater.* **18**, 2364–2375 (2006)
23. O.N. Krasnobaeva, I.P. Belomestnykh, G.V. Isagulyants, T.A. Nosova, T.A. Elizarova, T.D. Teplyakova, D.F. Kondakov, V.P. Danilov, Synthesis of complex hydroxo salts of magnesium, nickel, cobalt, aluminum, and bismuth and oxide catalysts on their base. *J. Inorg. Chem.* **52**, 141–146 (2007)
24. G.S. Zhang, J.H. Qu, H.J. Liu, R.P. Liu, R.C. Wu, Fe-Mn binary oxide adsorbent for effective arsenic removal. *Water Res.* **41**(6), 1921–1928 (2007)
25. H. Ye, F. Chen, Y. Sheng, G. Sheng, J. Fu, Adsorption of phosphate from aqueous solution onto modified palygorskites. *Sep. Purif. Technol.* **50**, 283–290 (2006)
26. Z. Talip, M. Eral, Ü. Hiçsönmez, Adsorption of thorium from aqueous solutions by perlite. *J. Environ. Radioact.* **100**(2), 139–143 (2009)
27. E.N. Mahmoud, F.Y. Fayed, K.M. Ibrahim, S. Jaafreh, Removal of cadmium, copper, and lead from water using biosorbent from treated olive mill solid residue. *Environ. Health Insights* **15**, 11786302211053176 (2021)
28. N. Soltanzadeh, A. Morsali, Sonochemical synthesis of a new nanostructures bismuth (III) su-pramolecular compound: new precursor for the preparation of bismuth(III) oxide nano rods and bismuth (III) iodide nano wires. *Ultrason. Sonochem.* **17**, 139–144 (2010)
29. P. Subrahmanyam, B. KrishnaPriya, B. Jayaraj, P. Chiranjeevi, Determination of Cd, Cr, Cu, Pb and Zn from various water samples with use of FAAS techniques after the solid phase extraction on rice bran. *Toxicol. Environ. Chem.* **90**(1), 97–106 (2008)
30. W.N. Nyairo, Y.R. Eker, C. Kowenje, I. Akin, H. Bingol, A. Tor, D.M. Onger, Efficient adsorption of lead (II) and copper (II) from aqueous phase using oxidized multiwalled carbon nanotubes/polypyrrole composite. *Sep. Sci. Technol.* **53**, 1498–1510 (2018)
31. M. Banerjee, R. KumarBasu, S.K. Das, Adsorptive removal of Cu (II) by pistachio shell: isotherm study, kinetic modelling and scaleup designing continuous mode. *Environ. Technol. Innov.* **15**, 100419 (2019)
32. N. Viswanathan, C.S. Sundaram, S. Meenak-shi, Sorption behaviour of fluoride on carboxylated cross-linked chitosan beads. *Colloids Surf. B* **68**(1), 48–54 (2009)
33. X. Wu, Y. Zhang, X. Dou, M. Yang, Fluoride removal performance of a novel Fe-Al-Ce trimetal oxide adsorbent. *Chemosphere* **69**, 1758–1764 (2007)
34. W. Ngeontae, W. Aeungmaitrepirom, T. Tuntulani, Chemically modified silica gel with aminothioamidoanthraquinone for solid phase extraction and preconcentration of Pb (II), Cu (II), Ni (II), Co (II) and Cd (II). *Talanta* **71**(3), 1075–1082 (2007)
35. M. Behpour, S.M. Ghoreishi, Z. NikkhahQamsari, M. Samiei, N. Soltani, Solid phase extraction of uranium by naphthalene-methyl-trioctylammonium chloride and arsenazo(III) adsorbent and subsequent spectrophotometric determination. *Chin. J. Chem.* **28**(8), 1457–1462 (2010)
36. C. Cui, H. Peng, Y. Zhang, K. Nan, M. He, B. Chen, B. Hu, Ti-containing mesoporous silica packed microcolumn separation/preconcentration combined with inductively coupled plasma-mass spectrometry for the determination of trace Cr, Cu, Cd and Pb in environmental samples. *J. Analyt. At. Spectrom.* **30**, 1386–1394 (2015)
37. J.S. Suleiman, B. Hu, H. Peng, C. Huang, Separation/preconcentration of trace amounts of Cr, Cu and Pb in environmental samples by magnetic solid-phase extraction with Bismuthiol-II-immobilized magnetic nanoparticles and their determination by ICP-OES. *Talanta* **77**, 1579–1583 (2009)
38. Ö. Yalçınkaya, O.M. Kalfa, A.R. Türker, Chelating agent free-solid phase extraction (CAF-SPE) of Co (II), Cu (II) and Cd (II) by new nano hybrid material ( $\text{ZrO}_2/\text{B}_2\text{O}_3$ ). *J. Hazard. Mater.* **195**, 332–339 (2011)

**Publisher's Note** Springer Nature remains neutral with regard to jurisdictional claims in published maps and institutional affiliations.

Springer Nature or its licensor holds exclusive rights to this article under a publishing agreement with the author(s) or other rightsholder(s); author self-archiving of the accepted manuscript version of this article is solely governed by the terms of such publishing agreement and applicable law.